Inorganic Chemistry

Article

pubs.acs.org/IC

Stannylenes: Structures, Electron Affinities, Ionization Energies, and Singlet–Triplet Gaps of SnX_2/SnXY and $XSnR/SnR_2/RSnR'$ Species (X; Y = H, F, Cl, Br, I, and R; R′ = CH_3, SiH_3, GeH_3, SnH_3)

Ashwini Bundhun,[†] Ponnadurai Ramasami,*[,†] Peter P. Gaspar,[‡] and Henry F. Schaefer, III*[,§]

[†]Computational Chemistry Group, Department of Chemistry, University of Mauritius, Réduit, Mauritius

[‡]Department of Chemistry, Washington University, Saint Louis, Missouri 63130, United States

[§]Center for Computational Quantum Chemistry, University of Georgia, Athens, Georgia 30602, United States

Supporting Information

ABSTRACT: Systematic computational studies of stannylene derivatives SnX_2/SnXY and $XSnR/SnR_2/RSnR'$ were carried out using density functional theory. The basis sets used for H, F, Cl, Br, C, Si, and Ge atoms are of double-ζ plus polarization quality with additional s- and p-type diffuse functions, denoted DZP++. For the iodine and tin atoms, the Stuttgart-Dresden basis sets, with relativistic small-core effective core potentials (ECP), are used. All geometries are fully optimized with three functionals (BHLYP, BLYP, and B3LYP). Harmonic vibrational wavenumber analyses are performed to evaluate zero-point energy corrections and to determine the nature of the stationary points located. Predicted are four types of neutral-anion separations, plus adiabatic ionization energies (E_{IE}) and singlet–triplet energy gaps ($\Delta E_{S\text{-}T}$). The dependence of all three energetic properties upon choice of substituent is remarkably strong. The $EA_{ad(ZPVE)}$ values (eV) obtained with the B3LYP functional range from 0.70 eV [$Sn(CH_3)_2$] to 2.36 eV [SnI_2]. The computed E_{IE} values lie between 7.33 eV [$Sn(SnH_3)_2$] and 11.15 eV [SnF_2], while the singlet–triplet splittings range from 0.60 eV [$Sn(SnH_3)_2$] to 3.40 eV [SnF_2]. The geometries and energetics compare satisfactorily with the few available experiments, while most of these species are investigated for the first time. Some unusual structures are encountered for the $SnXI^+$ (X = F, Cl, and Br) cations. The structural parameters and energetics are discussed and compared with the carbene, silylene, and germylene analogues.

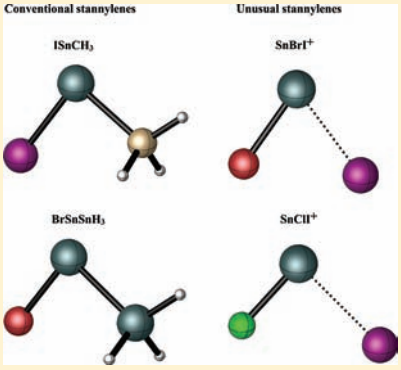

I. INTRODUCTION

The ultraprecision construction of semiconductors[1−3] and the exploration of stannylenes[4,5] with novel properties for microelectronic engineering[6] are important areas of research. These species play significant roles in chemical vapor deposition (CVD) processes.[7,8] Stannylenes have also proved to be important in understanding new organometallic chemistry, a pivotal contribution being Sekiguchi's work[9,10] on structure and bonding of distannenes. The use of diazomethylstannylene to synthesize a short-lived stannaacetylene is another important laboratory accomplishment.[11] A significant recent achievement is the preparation of a cyclic disilylated stannylene by Arp, Baumgartner, Marschner, and Müller.[12] There has also been special interest[13] in the related N,N′ germylenes. Even more recently, Wagler and co-workers[14] have reported a reaction sequence starting from $SnCl_2$ to synthesize hypercoordinate palladstanna (IV) octanes. An excellent 2002 review of stannylenes is that of Boganov and co-workers.[15] The recent finding that 1,1-disubstituted 1-stannacyclopent-3-enes are synthetically accessible,[16] and undergo clean extrusion of disubstituted stannylenes under both photochemical[17] and mild thermal[16] conditions holds promise that many of the species studied in this work will soon be realized experimentally and may well prove to be useful synthetic reagents.

Stannous dichloride[18−21] has been studied because of its unique industrial applications, as $SnCl_2$ plays an important role in the semiconductor gas sensor industry, specifically in CVD processes. Nasarenko et al.[22] deduced experimental bond lengths for a series of dihalogenated stannylenes, using a best fit of the electron diffraction data to a molecular potential function, yielding 2.338 Å ($SnCl_2$), 2.504 Å ($SnBr_2$), and 2.699 Å (SnI_2). The vertical ionization energy of $SnBr_2$ has been reported by different workers using photoelectron spectroscopy (PES). Experimental results reported by Novak and Potts,[23] Harris et al.,[24] and Evans and Orchard[25] were 9.83, 9.87 ± 0.05, and 9.85 ± 0.05 eV, respectively. Novak and Potts[23] also determined an experimental value for the vertical ionization energy of SnI_2 = 9.05 eV.

Perhaps the earliest (1980) theoretical study of SnH_2 was that of Olbrich.[26] He performed ab initio computations using double-ζ basis sets for the $^1A_1$ and $^3B_1$ states of SnH_2 and reported the geometrical parameters for the $^1A_1$ state as r_e = 1.756 Å, θ_e = 92.7° and the lowest lying $^3B_1$ state as r_e = 1.707 Å, θ_e = 118.2°, and $\Delta E_{S\text{-}T}$ = 10.5 kcal mol^{-1}. In the same decade, Balasubramanian[27,28] carried out more detailed systematic

Received: June 29, 2011
Published: January 3, 2012

   dx.doi.org/10.1021/ic201389y | Inorg. Chem. 2012, 51, 851–863

theoretical studies on the low-lying states of SnH_2 using complete active space MC SCF (CAS SCF) followed by full-second order configuration interaction (CI) computations and reported the bond distances and angles as r_e = 1.803 Å, θ_e = 91.7° ($^1A_1$) and r_e = 1.731 Å, θ_e = 117.8° ($^3B_1$), $\Delta E_{S\text{-}T}$ = 22.5 kcal mol^{-1}. Using the second-order CI method the predicted SnH_2 equilibrium bond lengths and bond angles are r_e = 1.780 Å, θ_e = 91.6° ($^1A_1$) and r_e = 1.719 Å, θ_e = 118.8° ($^3B_1$), $\Delta E_{S\text{-}T}$ = 23.8 kcal mol^{-1}.

Turning to the dihalostannylenes, in 1986 Ricart, Rubio, and Illas[29] used the SCF and CI levels, with nonempirical pseudopotentials and double-ζ plus polarization quality basis sets, to compute geometries for the neutrals $^1A_1$ SnX_2 and cations $^2A_1$ SnX_2^+ (X = Cl, Br, and I), respectively. The predicted Sn−X (X = Cl, Br, and I) bond lengths were 2.352 Å, 2.516 Å, and 2.746 Å at the SCF level and 2.362 Å, 2.530 Å, and 2.771 Å at the CI level, respectively. For their cationic counterparts the Sn−X bond lengths were reported at 2.242 Å, 2.404 Å, and 2.631 Å (SCF) and 2.278 Å, 2.496 Å, and 2.682 Å (CI). In 1994 Balasubramanian[30] predicted spectroscopic properties, ionization energies, dissociation energies, and singlet−triplet gaps for SnX_2 (X = Cl, Br, and I) using complete active space self-consistent field (CAS SCF) followed by multireference single plus double configuration interaction (MRSDCI). The theoretical $^1A_1$−$^3B_1$ energy splittings were reported to be 60.0 kcal mol^{-1} for $SnCl_2$, 55.5 kcal mol^{-1} for $SnBr_2$, and 47.1 kcal mol^{-1} for SnI_2. In 1999, Escalante et al.[31] tested the performance of density functional theory (DFT) for the SnX_2 species (X = F, Cl, Br, and I) considering three different exchange correlation functionals with the ECPs of the Stuttgart/Bonn group. Finally (2003) Szabados and Hargittai[32] performed systematic theoretical studies on the dihydride SnH_2 and dihalides SnX_2 (X = F, Cl, Br, and I) and obtained the singlet−triplet energy separations using the CCSD-(T) method.

This research systematically explores the abilities of the neutral ground state stannylenes to bind an extra electron, with additional insights into their ionization energies and singlet−triplet gaps. Most of the tin congeners in this series are not known experimentally and have not been studied theoretically to date. The predicted results may be used as groundwork for the quest of new stannylenes and encouraging future experiments. Further, the results obtained are analyzed and compared to their carbene,[33,34] silylene,[35] and germylene[36] analogues, and trends for the geometrical parameters and energetics are established.

II. THEORETICAL METHODS

All geometries are fully optimized using the Gaussian 03 program.[37] Three density functionals, namely, BHLYP, BLYP, and B3LYP, are used. BHLYP is an HF/DFT hybrid method comprising the Becke (B)[38] half and half exchange functional (H)[39] and the Lee, Yang and Parr (LYP)[40] nonlocal correlation functional. The B3LYP method combines Becke's three parameter exchange functional (B3) with the LYP correlation functional. BLYP is a pure DFT method, comprised of Becke's (B) exchange functional plus the LYP correlation. In all cases a very tight convergence (10^{-6}) and extended integration grid (199,974) criteria were applied. All ground state structures are characterized as minima on their corresponding potential energy surfaces by performing harmonic vibrational wavenumber analyses. Natural bond orbital analyses were carried out with NBO 3.1[41] linked through the Gaussian package.

Double-ζ basis sets with polarization and diffuse functions, denoted as DZP++, are used for the following atoms: H, F, Cl, Br, C, Si, and Ge. The valence basis sets used for iodine and tin are coupled with a fully relativistic small-core effective core potential.[42] The double-ζ basis sets were constructed by augmenting the Huzinaga−Dunning−Hay[43−45] sets of contracted Gaussian functions with one set of p polarization functions for each H atom and one set of d polarization functions for each heavy atom, respectively [α_p(H) = 0.75, α_d(C) = 0.75, α_d(F) = 1.0, α_d(Si) = 0.5]. Basis functions for chlorine begin with the Ahlrichs standard double-ζ sp set[46] with one set of d-like polarization functions [α_d(Cl) = 0.75]. For bromine, the Ahlrichs standard double-ζ spd set was appended with d polarization functions, α = 0.389. The above basis sets were further augmented with diffuse functions, where each heavy atom received one additional s-type and p-type functions. The H atom basis set is appended with one diffuse s function. The diffuse functions were determined in an even-tempered fashion following the prescription of Lee and Schaefer,[47]

$$\alpha_{\text{diffuse}} = \frac{1}{2}\left(\frac{\alpha_1}{\alpha_2} + \frac{\alpha_2}{\alpha_3}\right)\alpha_1$$

where α_1, α_2, and α_3 are the three smallest Gaussian orbital exponents of the s- or p-type primitive functions of a given atom ($\alpha_1 < \alpha_2 < \alpha_3$). Thus α_s(H) = 0.04415, α_s(C) = 0.04302, α_p(C) = 0.03629, α_s(F) = 0.1049, α_p(F) = 0.0826, α_s(Si) = 0.02729, α_p(Si) = 0.025, α_s(Cl) = 0.05048, α_p(Cl) = 0.05087, α_s(Br) = 0.0469096, and α_p(Br) = 0.0465342.

The DZP++ basis set for germanium was constructed from the Schafer−Horn−Ahlrichs double-ζ spd set plus a set of five pure d-type polarization functions with α_d(Ge) = 0.246, and augmented by a set of sp diffuse functions with α_s(Ge) = 0.024434 and α_p(Ge) = 0.023059.[46] The overall contraction scheme for the basis sets is H(5s1p/3s1p), C(10s6p1d/5s3p1d), F(10s6p1d/5s3p1d), Si(13s9p1d/7s5p1d), Cl-(13s9p1d/7s5p1d), Ge(15s12p6d/9s7p3d), and Br(15s12p6d/9s7p3d).

The four forms of the neutral-anion energy differences are evaluated as follows:

The adiabatic electron affinities:

$$\text{EA}_{\text{ad}} = E(\text{optimized neutral}) - E(\text{optimized anion}) \quad (1)$$

Additionally, zero-point vibrational energies (ZPVE) are evaluated for each system. The ZPVE corrected adiabatic electron affinities $\text{EA}_{\text{ad(ZPVE)}}$ are reported as follows:

$$\text{EA}_{\text{ad(ZPVE)}} = [E(\text{optimized neutral}) + \text{ZPVE}_{\text{neutral}}] - [E(\text{optimized anion}) + \text{ZPVE}_{\text{anion}}] \quad (2)$$

Vertical electron affinities:

$$\text{EA}_{\text{vert}} = E(\text{optimized neutral}) - E(\text{anion at optimized neutral geometry}) \quad (3)$$

Vertical detachment energies:

$$\text{VDE} = E(\text{neutral at optimized anion geometry}) - E(\text{optimized anion}) \quad (4)$$

The ionization energies:

$$E_{\text{IE}} = E(\text{optimized cation}) - E(\text{optimized neutral}) \quad (5)$$

Each singlet−triplet splitting is predicted as the energy difference between the neutral ground state and its lowest triplet state.

III. RESULTS

This section discusses the geometries, electron affinities, adiabatic ionization energies, and singlet−triplet gaps obtained, including comparisons with the few available theoretical and experimental findings for stannylene derivatives. All equilibrium geometries are presented in Supporting Information except for Figures 1−8.

A. SnH_2. From Figure 1 the differences in the geometrical parameters between the neutral and the ground state anion

dx.doi.org/10.1021/ic201389y | Inorg. Chem. 2012, 51, 851−863

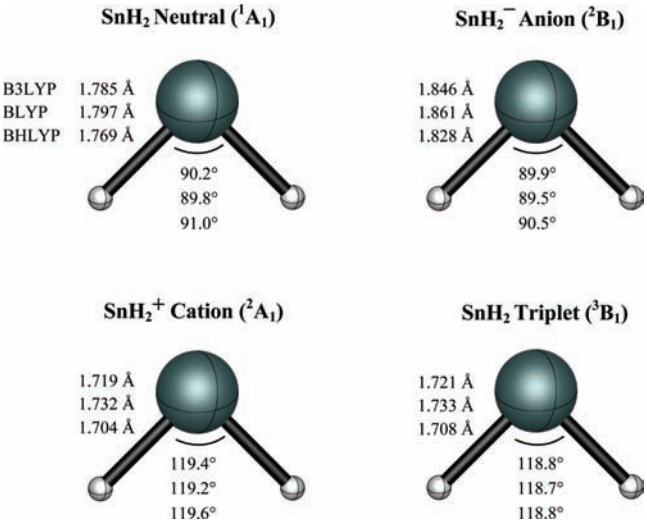

Figure 1. Equilibrium geometries for the $^1A_1$ ground state of SnH_2, $^2B_1$ ground state of the SnH_2^- anion, $^2A_1$ ground state of the SnH_2^+ cation, and $^3B_1$ excited state of neutral SnH_2.

show an increase in the Sn−H bond length of 0.064 Å (BLYP), with a tiny decrease in the divalent angle of 0.3°. The B3LYP harmonic vibrational wavenumbers for SnH_2 ($^1A_1$) 1674 cm^{-1} (antisymmetric stretching) and 1684 cm^{-1} (symmetric stretching) show excellent agreement with the experimental values reported by Wang and Andrews.[48,49] Supporting Information, Table S1 presents the theoretical harmonic vibrational wavenumbers (cm^{-1}) for SnX_2 (X = H, F, Cl, Br, and I) species with C_{2v} symmetry, and Table 1 presents the frontier molecular orbitals for the neutral ground state $^1A_1$ SnX_2 (C_{2v}) molecules (X = H, F, Cl, Br, and I).

Between the ground state neutral and cation there is a decrease in the bond length of 0.065 Å (BHLYP), while the bond angle is predicted to increase by 28.6°. Between the neutral ground state and the lowest lying triplet state of SnH_2 there is a decrease in the bond length of 0.061 Å accompanying a large increase in the bond angle of 27.8° (BHLYP). Compared to the $^1A_1$ SnH_2 ground state, the larger bond angles for $^2A_1$ SnH_2^+ and $^3B_1$ SnH_2 are due to the loss of an electron from the lone-pair a_1 orbital, which strongly favors bent geometries. For each species the theoretical adiabatic electron affinity EA_{ad} and zero-point corrected $EA_{ad(ZPVE)}$ are presented in Table 2 and the vertical electron affinity EA_{vert}, and vertical detachment energy VDE are reported in Supporting Information, Tables S2−S3. Tables 3 and 4 present

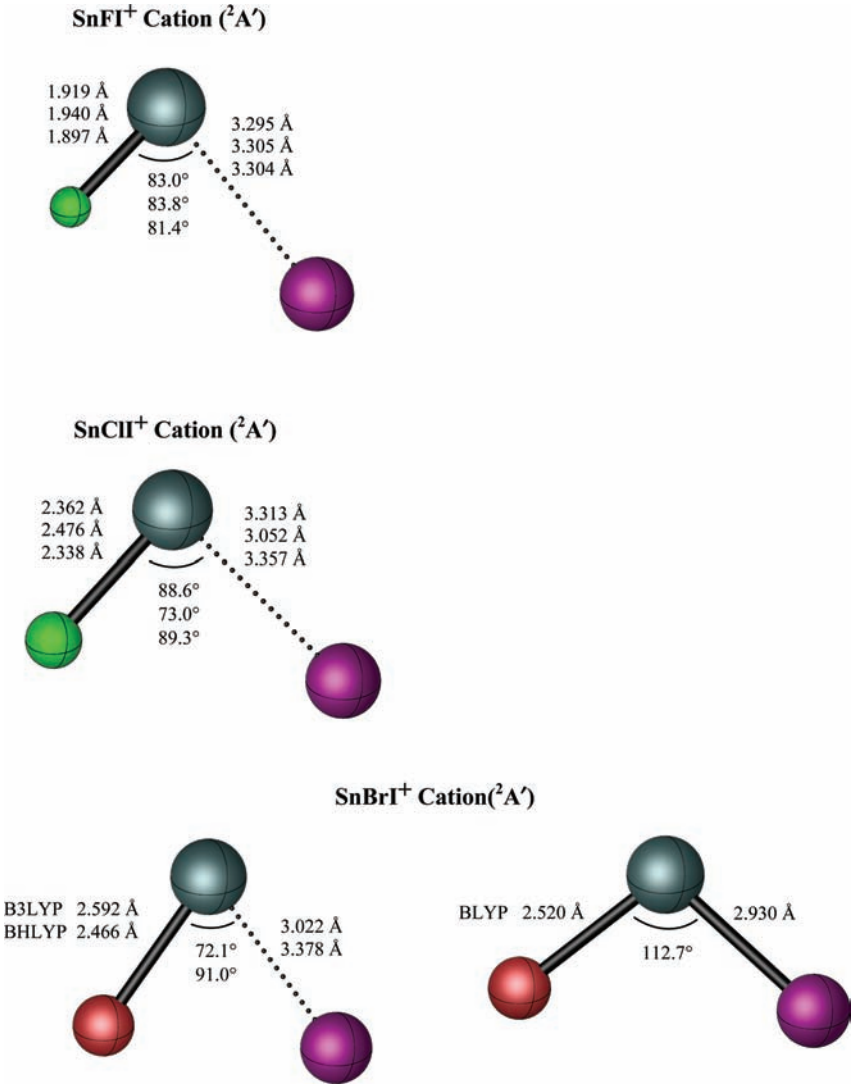

Figure 2. Equilibrium geometries for the $^2A'$ ground state of $SnFI^+$, $SnClI^+$, $SnBrI^+$ cations.

dx.doi.org/10.1021/ic201389y | Inorg. Chem. 2012, 51, 851−863

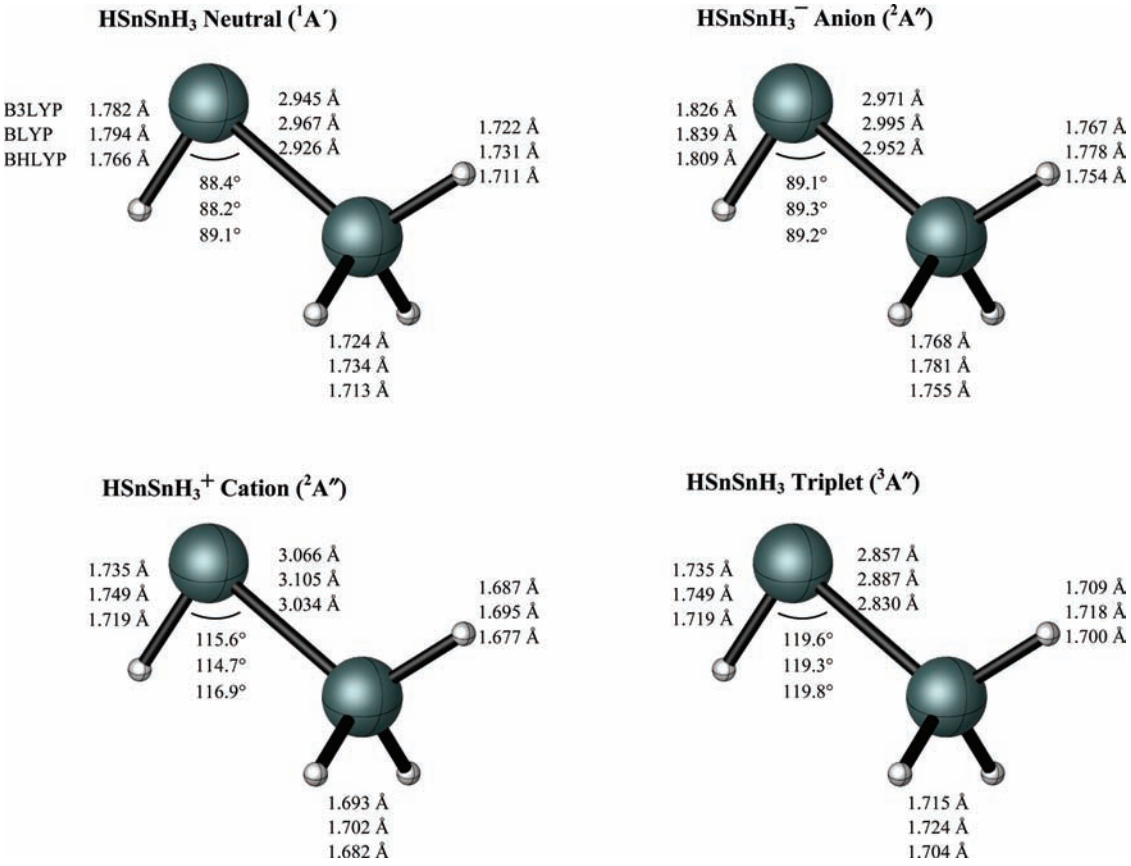

Figure 3. Equilibrium geometries for the $^1A'$ ground state of $HSnSnH_3$, $^2A''$ ground state of the $HSnSnH_3^-$ anion, $^2A''$ ground state of the $HSnSnH_3^+$ cation, and $^3A''$ excited state of neutral $HSnSnH_3$.

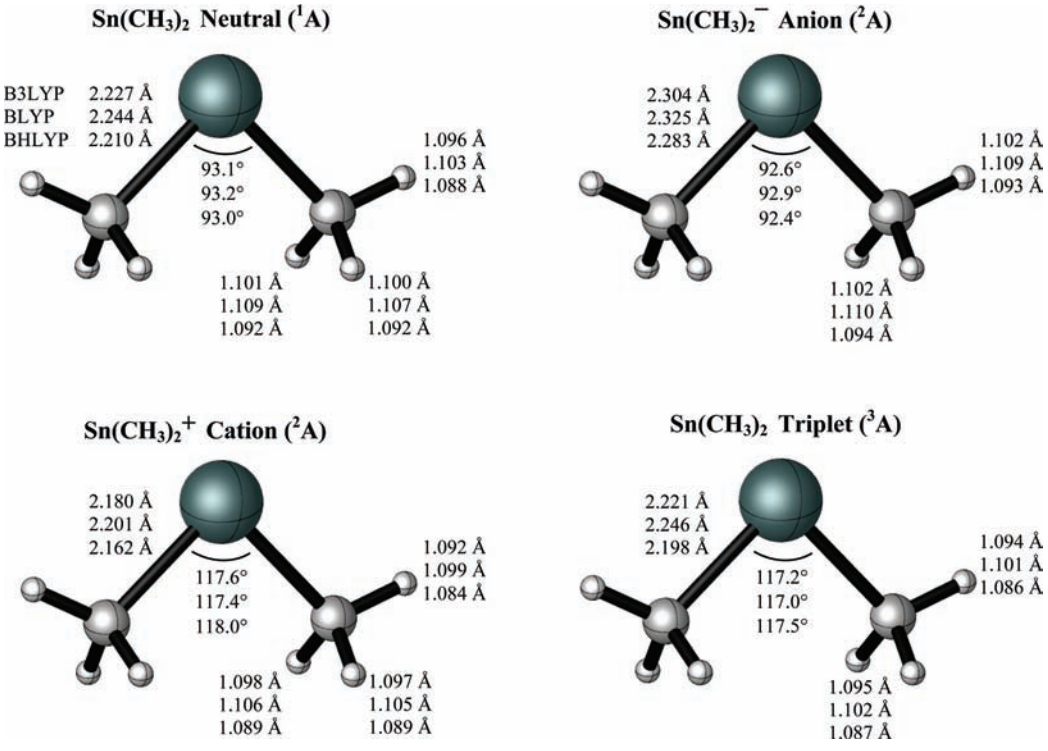

Figure 4. Equilibrium geometries for the ^1A ground state of $Sn(CH_3)_2$, ^2A ground state of the $Sn(CH_3)_2^-$ anion, ^2A ground state of the $Sn(CH_3)_2^+$ cation, and ^3A excited state of neutral $Sn(CH_3)_2$.

the ionization energies (eV) and singlet−triplet gaps (eV and kcal mol^{-1}), respectively. For SnH_2, the $EA_{ad(ZPVE)}$ values fall in the range 0.80 (BLYP) to 0.97 eV (B3LYP). The predicted EA_{vert} and VDE range from 0.73 to 0.90 eV and 0.80 to 0.97 eV, respectively, in the

dx.doi.org/10.1021/ic201389y | Inorg. Chem. 2012, 51, 851−863

Table 1. Frontier Molecular Orbitals (HOMOs and LUMOs), LUMO−HOMO Gaps (eV), Dipole Moments (Debye), and Rotational Constants (GHz) for the Neutral Ground State $^1A_1$ SnX_2 (C_{2v}) Molecules (X = H, F, Cl, Br, and I) with the B3LYP Functional

	HOMO	LUMO	LUMO-HOMO Gap (eV)	Dipole moment (Debye)	Rotational constants (GHz)
SnH_2			3.23	0.70	A: 160.84 B: 156.77 C: 79.39
SnF_2			5.45	4.41	A: 10.09 B: 6.26 C: 3.86
$SnCl_2$	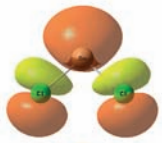	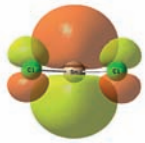	4.33	4.32	A: 4.57 B: 2.09 C: 1.43
$SnBr_2$	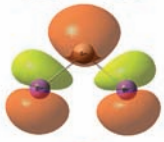	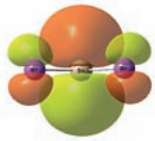	3.96	3.70	A: 2.70 B: 0.81 C: 0.63
SnI_2	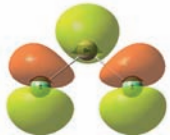	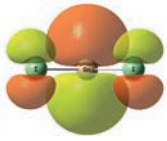	3.27	3.77	A: 1.95 B: 0.41 C: 0.34

order BLYP < BHLYP < B3LYP. The E_{IE} for SnH_2 ranges from 8.37 (BHLYP) to 8.55 eV (B3LYP). The theoretical $^1A_1 - {}^3B_1$ energy difference of 23.8 kcal mol^{-1} reported by Balasubramanian[50] is found to be consistent with the energy separation of 24.8 kcal mol^{-1} obtained here with the BHLYP functional.

B. SnF_2. The infrared spectra of the matrix isolated tin difluoride reported by Hauge, Hastie, and Margrave[51] (Ne: ν_1 = 605 cm^{-1}, ν_3 = 584 cm^{-1}, ν_2 = 201 cm^{-1}; Ar: ν_1 = 593 cm^{-1}, ν_3 = 571 cm^{-1}, ν_2 = 197 cm^{-1}) are relatively close to our predicted values in Supporting Information, Table S1. The bent symmetric SnF_2 molecule has three infrared active fundamentals, two stretching modes, and one bending mode. The earlier experimental ground state tin difluoride molecule band at 180 cm^{-1} for the bending wavenumber[52] was assigned using ultraviolet absorption spectra. The geometrical changes accompanying the addition of an extra electron to SnF_2 are an increase of 0.118 Å and a decrease of 0.2° (B3LYP) in the bond length and bond angle, respectively. Structural differences between the neutral SnF_2 and the SnF_2^+ cation correspond to a decrease in the Sn−F bond length by 0.066 Å with a large increase in the F−Sn−F bond angle of 20.5° predicted by the B3LYP functional. The equilibrium geometry of the $^3B_1$ state reveals a decrease in the bond length by 0.008 Å (BHLYP), accompanying a large opening of the bond angle by 20.4°. Comparing the neutral $^1A_1$ SnF_2 to SnH_2 reveals that substitution of the hydrogen atoms by fluorine shows an increase in the bond distance by 0.192 Å and divalent angle by 6.5° (BLYP). A similar increase is observed for their anionic counterparts. It is observed that the fluorine atoms increase the $EA_{ad(ZPVE)}$, EA_{vert}, and VDE by 0.22, 0.09, and 0.42 eV (BHLYP), respectively, compared to SnH_2. The E_{IE} value of 11.11 eV at the BHLYP level shows perfect agreement with Novak's and Potts's experimental value of 11.10 eV,[53] and satisfactory agreement with the older value of 11.5 ± 0.2 eV.[54,55] An experimentally determined SnF_2 vertical ionization energy of 11.5 eV was reported by Novak and Potts.[53] Dai and co-workers[56] reported theoretical adiabatic E_{IE} values of 9.74 eV (CASMCSCF), 10.47 eV (MRSDCI), and 10.54 eV (MRSDCI+Q).

C. $SnCl_2$. There is an increase in the Sn−Cl bond distance of 0.176 Å from the neutral to the anion, with a concomitant increase in the Cl−Sn−Cl bond angle of 2.5° (B3LYP). Compared to the neutral ground state, the $^2A_1$ cation geometry of $SnCl_2^+$ shows a decrease from the singlet Sn−Cl bond length by 0.087 Å, with a correspondingly large increase in the bond angle of 20.4°. There is an appreciable increase in the Cl−Sn−Cl bond angle of 22.1° from the $^1A_1 \rightarrow {}^3B_1$ electronic excitation, with only a slight decrease in the Sn−Cl bond length of 0.004°. The geometries of the neutral ground state $^1A_1$ $SnCl_2$ with Sn−Cl bond lengths of 2.357 Å (CCSD(T)/EC) and 2.380 Å (CCSD(T)/ST) from Szabados and Hargittai[32] are shorter than the BHLYP bond distance of 2.424 Å. The experimental electron affinity for $SnCl_2$ ($\tilde{X}^1A_1$) + $e^- \leftarrow SnCl_2^-$ ($\tilde{X}$ $^2B_1$) is 1.568 ± 0.007 eV,[21] less than our $EA_{ad(ZPVE)}$ values of 1.92 eV (BHLYP), 1.70 eV (BLYP), and 1.93 eV (B3LYP). Our theoretically predicted $EA_{ad(ZPVE)}$ = 1.70 eV (BLYP) is greater than the earlier experimental value EA = 1.04 eV reported by Pabst et al.[57] Substitution of the hydrogen atoms by chlorine in SnH_2 increases the $EA_{ad(ZPVE)}$, EA_{vert}, and VDE by 1.07, 0.89, and 1.34 eV, respectively, with the BHLYP functional. Lee et al.[20] established the first $E_{IE}(SnCl_2)$ = 10.09 ± 0.01 eV which is consistent to our BHLYP value of 10.16 eV. There is a significant increase ($SnH_2 \rightarrow SnCl_2$) in the E_{IE} by 1.79 eV along with an increase in the singlet−triplet gap of 1.55 eV. Several workers have reported

dx.doi.org/10.1021/ic201389y | Inorg. Chem. 2012, 51, 851−863

Table 2. Stannylene Adiabatic Electron Affinities EA_{ad} and Zero-Point Corrected $EA_{ad(ZPVE)}$ Values (in Parentheses) in Electron Volts (eV)[a]

	BHLYP		BLYP		B3LYP		GeR_2	SiR_2	CR_2
SnH_2	0.81	(0.85)	0.77	(0.80)	0.93	(0.97)	1.03	1.02	0.6520 ± 0.0060[64]
SnF_2	1.06	(1.07)	0.95	(0.97)	1.14	(1.16)	0.87	0.41	<1.30 ± 0.80[65]
SnCl_2	1.91	(1.92)	1.69	(1.70)	1.92	(1.93)	1.66	1.50	1.590 ± 0.070[66]
SnBr_2	1.96	(1.97)	1.73	(1.74)	1.97	(1.98)	1.82	1.72	1.880 ± 0.070[66]
SnI_2	2.42	(2.43)	2.06	(2.07)	2.35	(2.36)	2.07		2.090 ± 0.070[66]
SnHF	0.96	(0.99)	0.88	(0.91)	1.06	(1.09)	0.98	0.76	0.5570 ± 0.0050[67]
SnHCl	1.43	(1.45)	1.29	(1.31)	1.49	(1.52)	1.39	1.29	1.2130 ± 0.0050[67]
SnHBr	1.47	(1.49)	1.33	(1.35)	1.53	(1.56)	1.47	1.41	
SnHI	1.73	(1.75)	1.52	(1.54)	1.75	(1.77)	1.61		
SnFCl	1.52	(1.53)	1.35	(1.36)	1.57	(1.58)	1.30	0.99	
SnFBr	1.56	(1.57)	1.39	(1.40)	1.61	(1.62)	1.40	1.14	
SnFI	1.84	(1.85)	1.60	(1.61)	1.84	(1.85)	1.56		
SnClBr	1.93	(1.94)	1.71	(1.72)	1.95	(1.96)	1.75		
SnClI	2.17	(2.18)	1.88	(1.89)	2.15	(2.15)	1.88		
SnBrI	2.19	(2.20)	1.90	(1.90)	2.16	(2.17)	1.95		
H**Sn**CH_3	0.68	(0.71)	0.65	(0.69)	0.80	(0.84)	0.71	0.65	
F**Sn**CH_3	0.80	(0.82)	0.74	(0.76)	0.90	(0.92)	0.66	0.40	
Cl**Sn**CH_3	1.22	(1.24)	1.11	(1.13)	1.29	(1.32)	1.09	1.03	
Br**Sn**CH_3	1.27	(1.29)	1.16	(1.18)	1.34	(1.36)	1.19	1.09	
I**Sn**CH_3	1.53	(1.55)	1.35	(1.36)	1.56	(1.58)	1.33		
H**Sn**SiH_3	1.39	(1.43)	1.36	(1.39)	1.52	(1.55)	1.51		
F**Sn**SiH_3	1.51	(1.54)	1.44	(1.47)	1.61	(1.64)	1.47		
Cl**Sn**SiH_3	1.86	(1.88)	1.73	(1.75)	1.92	(1.95)	1.80		
Br**Sn**SiH_3	1.88	(1.90)	1.75	(1.77)	1.95	(1.97)	1.87		
I**Sn**SiH_3	2.10	(2.12)	1.90	(1.92)	2.13	(2.14)	1.98		
H**Sn**GeH_3	1.42	(1.46)	1.41	(1.45)	1.56	(1.59)	1.55	1.55	
F**Sn**GeH_3	1.54	(1.57)	1.49	(1.52)	1.65	(1.68)	1.50	1.31	
Cl**Sn**GeH_3	1.87	(1.90)	1.77	(1.79)	1.95	(1.98)	1.83	1.77	
Br**Sn**GeH_3	1.89	(1.92)	1.78	(1.81)	1.97	(1.99	1.89	1.86	
I**Sn**GeH_3	2.11	(2.13)	1.94	(1.96)	2.15	(2.17)	2.00		
H**SnSn**H_3	1.58	(1.62)	1.52	(1.56)	1.69	(1.73)			
F**SnSn**H_3	1.70	(1.74)	1.61	(1.65)	1.79	(1.83)			
Cl**SnSn**H_3	2.03	(2.06)	1.89	(1.92)	2.09	(2.12)			
Br**SnSn**H_3	2.05	(2.08)	1.90	(1.93)	2.11	(2.13)			
I**SnSn**H_3	2.26	(2.29)	2.05	(2.08)	2.28	(2.31)			
Sn$(CH_3)_2$	0.52	(0.56)	0.52	(0.56)	0.66	(0.70)	0.46	0.38	
Sn$(SiH_3)_2$	1.78	(1.82)	1.75	(1.78)	1.90	(1.94)	1.90	-	
Sn$(GeH_3)_2$	1.82	(1.86)	1.82	(1.86)	1.96	(2.00)	1.95	1.98	
Sn$(SnH_3)_2$	2.13	(2.17)	2.05	(2.09)	2.23	(2.27)			
CH_3**Sn**SiH_3	1.21	(1.24)	1.19	(1.22)	1.33	(1.36)	1.22		
CH_3**Sn**GeH_3	1.24	(1.27)	1.24	(1.28)	1.37	(1.41)	1.26	1.23	
CH_3**SnSn**H_3	1.41	(1.45)	1.37	(1.41)	1.52	(1.56)			
SiH_3**Sn**GeH_3	1.80	(1.84)	1.78	(1.82)	1.93	(1.97)			
SiH_3**SnSn**H_3	1.96	(2.00)	1.91	(1.94)	2.07	(2.11)			
GeH_3**SnSn**H_3	1.98	(2.02)	1.94	(1.98)	2.09	(2.14)			

[a]The boldface **Sn** designates the divalent tin atom. The last three columns report theoretical results for germylene,[36] silylene,[35] and experimental results for carbene derivatives.

experimental $E_{IE(vertical)}$ values using PES at 10.31,[23] 10.37 ± 0.05,[24] and 10.31 ± 0.05 eV.[25]

D. $SnBr_2$. An experimentally determined equilibrium r_e(Sn−Br) = 2.504 Å bond distance and θ_e(Br−Sn−Br) = 98.6 ± 0.7° reported by Nasarenko et al.[22] is consistent with our predicted BHLYP geometry of 2.568 Å and 99.0° for the neutral $^1A_1$ $SnBr_2$. The computed Sn−Br bond length of 2.496 Å of Ricart et al.[29] fits perfectly with our equilibrium bond length of 2.497 Å for the $SnBr_2^+$ cation, while their divalent bond angle is larger by nearly 1.5°. The optimized geometry of the lowest triplet state $^3B_1$ $SnBr_2$, shows a decrease in the Sn−Br distance by 0.015 Å (BHLYP) with respect to its corresponding neutral singlet state. An experimental EA = 1.33 eV was reported by Margrave and Franklin[57] from the electron impact appearance energy (EIAE). Our theoretical value (BLYP) for the adiabatic E_{IE} = 9.33 eV is found to be a bit higher than the Novak and Potts[23] value of 9.0 eV from PES. Other reported values of the $SnBr_2$ ionization energy are 10.6 ± 0.2[58] and 10.0 ± 0.4 eV[59] from the EI technique.

E. SnI_2. The BHLYP functional results for the $^1A_1$ Sn−I bond distances of 2.831 Å and bond angle 101.2° are in close agreement with Szabados and Hargittai's results.[32] The iodine substitutions raise the $EA_{ad(ZPVE)}$, EA_{vert}, and VDE by 1.27, 1.13,

dx.doi.org/10.1021/ic201389y | Inorg. Chem. 2012, 51, 851−863

Table 3. Ionization Energies (in eV)

	BHLYP	BLYP	B3LYP
SnH_2	8.37	8.40	8.55
SnF_2	11.11	10.87	11.15
$SnCl_2$	10.16	9.88	10.17
$SnBr_2$	9.62	9.33	9.63
SnI_2	9.21	8.90	9.21
SnHF	9.34	9.24	9.46
SnHCl	9.17	9.00	9.25
SnHBr	8.95	8.77	9.02
SnHI	8.87	8.63	8.90
SnFCl	10.55	10.30	10.58
SnFBr	10.19	9.94	10.22
SnFI	9.20	9.23	9.40
SnClBr	9.87	9.59	9.88
SnClI	9.20	9.10	9.37
SnBrI	9.08	9.06	9.17
$HSnCH_3$	7.86	7.84	8.01
$FSnCH_3$	8.57	8.48	8.70
$ClSnCH_3$	8.58	8.40	8.65
$BrSnCH_3$	8.42	8.22	8.48
$ISnCH_3$	8.39	8.13	8.41
$HSnSiH_3$	7.74	7.74	7.91
$FSnSiH_3$	8.09	7.99	8.20
$ClSnSiH_3$	8.14	7.97	8.21
$BrSnSiH_3$	6.35	7.85	8.10
$ISnSiH_3$	8.05	7.83	8.09
$HSnGeH_3$	7.71	7.71	7.87
$FSnGeH_3$	8.03	7.93	8.14
$ClSnGeH_3$	8.08	7.92	8.15
$BrSnGeH_3$	7.97	7.80	8.04
$ISnGeH_3$	8.01	7.78	8.04
$HSnSnH_3$	7.55	7.55	7.71
$FSnSnH_3$	7.78	7.68	7.89
$ClSnSnH_3$	7.82	7.67	7.90
$BrSnSnH_3$	7.73	7.57	7.81
$ISnSnH_3$	7.78	7.58	7.83
$Sn(CH_3)_2$	7.47	7.40	7.60
$Sn(SiH_3)_2$	7.39	7.38	7.56
$Sn(GeH_3)_2$	7.36	7.35	7.52
$Sn(SnH_3)_2$	7.15	7.17	7.33
CH_3SnSiH_3	7.37	7.33	7.52
CH_3SnGeH_3	7.35	7.32	7.50
CH_3SnSnH_3	7.20	7.18	7.35
SiH_3SnGeH_3	7.38	7.36	7.54
SiH_3SnSnH_3	7.26	7.26	7.43
GeH_3SnSnH_3	7.25	7.25	7.42

Table 4. Singlet-Triplet Gaps[a]

	BHLYP		BLYP		B3LYP	
SnH_2	1.07	(24.8)	1.60	(37.0)	1.13	(26.2)
SnF_2	3.37	(77.8)	3.38	(78.0)	3.40	(78.5)
$SnCl_2$	2.62	(60.4)	2.68	(61.7)	2.68	(61.7)
$SnBr_2$	2.38	(54.8)	2.43	(56.0)	2.43	(56.0)
SnI_2	1.92	(44.2)	2.06	(47.4)	2.02	(46.6)
SnHF	1.88	(43.4)	1.94	(44.8)	1.94	(44.7)
SnHCl	1.72	(39.8)	1.79	(41.4)	1.78	(41.1)
SnHBr	1.66	(38.3)	1.73	(39.9)	1.72	(39.6)
SnHI	1.55	(35.7)	1.64	(37.7)	1.62	(37.3)
SnFCl	2.97	(68.6)	3.00	(69.2)	3.01	(69.5)
SnFBr	2.82	(64.9)	2.84	(65.6)	2.86	(65.8)
SnFI	2.48	(57.2)	2.58	(59.4)	2.56	(59.1)
SnClBr	2.49	(57.5)	2.55	(58.7)	2.55	(58.7)
SnClI	2.22	(51.3)	2.33	(53.8)	2.31	(53.3)
SnBrI	2.14	(49.2)	2.23	(51.5)	2.22	(51.1)
$HSnCH_3$	1.15	(26.4)	1.70	(39.3)	1.20	(27.7)
$FSnCH_3$	1.90	(43.8)	1.94	(44.6)	1.94	(44.8)
$ClSnCH_3$	1.76	(40.6)	1.80	(41.5)	1.80	(41.6)
$BrSnCH_3$	1.70	(39.3)	1.74	(40.0)	1.74	(40.2)
$ISnCH_3$	1.60	(36.9)	1.65	(38.0)	1.65	(38.1)
$HSnSiH_3$	0.80	(18.5)	0.93	(21.4)	0.89	(20.4)
$FSnSiH_3$	1.34	(30.9)	1.42	(32.7)	1.40	(32.3)
$ClSnSiH_3$	1.22	(28.2)	1.32	(30.4)	1.30	(29.9)
$BrSnSiH_3$	1.19	(27.5)	1.28	(29.6)	1.26	(29.2)
$ISnSiH_3$	1.11	(25.6)	1.22	(28.2)	1.19	(27.5)
$HSnGeH_3$	0.86	(19.8)	0.98	(22.5)	0.94	(21.7)
$FSnGeH_3$	1.38	(31.8)	1.46	(33.6)	1.44	(33.2)
$ClSnGeH_3$	1.26	(29.1)	1.35	(31.1)	1.33	(30.7)
$BrSnGeH_3$	1.23	(28.4)	1.32	(30.4)	1.30	(29.9)
$ISnGeH_3$	1.15	(26.5)	1.25	(28.8)	1.23	(28.3)
$HSnSnH_3$	0.76	(17.5)	0.90	(20.7)	0.85	(19.6)
$FSnSnH_3$	1.20	(27.7)	1.30	(30.0)	1.28	(29.4)
$ClSnSnH_3$	1.09	(25.1)	1.20	(27.7)	1.17	(27.0)
$BrSnSnH_3$	1.06	(24.5)	1.17	(27.1)	1.15	(26.4)
$ISnSnH_3$	0.98	(22.6)	1.11	(25.6)	1.07	(24.8)
$Sn(CH_3)_2$	1.25	(28.8)	1.29	(29.8)	1.29	(29.8)
$Sn(SiH_3)_2$	0.58	(13.4)	0.73	(16.9)	0.69	(15.8)
$Sn(GeH_3)_2$	0.68	(15.6)	0.81	(18.7)	0.77	(17.8)
$Sn(SnH_3)_2$	0.47	(10.9)	0.66	(15.2)	0.60	(13.8)
CH_3SnSiH_3	0.87	(20.0)	0.97	(22.3)	0.94	(21.7)
CH_3SnGeH_3	0.93	(21.3)	1.02	(23.6)	1.00	(23.0)
CH_3SnSnH_3	0.81	(18.8)	0.93	(21.6)	0.90	(20.7)
SiH_3SnGeH_3	0.63	(14.6)	0.77	(17.8)	0.73	(16.8)
SiH_3SnSnH_3	0.53	(12.2)	0.70	(16.1)	0.64	(14.8)
GeH_3SnSnH_3	0.58	(13.4)	0.74	(17.0)	0.69	(15.9)

[a] In eV; kcal mol^{-1} in parentheses.

and 1.49 eV (BLYP), respectively, compared to SnH_2. Using the electron impact appearance energy (EIAE) technique, Pabst and co-workers[57] reported the electron affinity for SnI_2 as 1.74 eV. This value lies below our predicted value of 2.07 eV (BLYP). The EA_{vert} and VDE values range from 1.86−2.20 eV and 2.29−2.68 eV, with BLYP and BHLYP as the lower and upper boundaries, respectively. The incremental corrections to the electron affinities for the disubstituted SnX_2 (X = F, Cl, Br, and I) series, in going from H → F → Cl → Br → I are 0.19, 0.77, 0.05, and 0.38 eV, respectively (B3LYP). The experimental E_{IE} results from the PES technique are reported as 8.9 eV[23] and 9.8 ± 0.2 eV,[58] and the result obtained using the EI technique was 8.8 ± 0.1 eV,[60] in close agreement with our BLYP value of 8.90 eV. The singlet−triplet splitting of 47.4 kcal mol^{-1} (BLYP) is consistent with the theoretical value, 48.0 kcal mol^{-1} obtained at the CCSD(T)/ST level of theory. Supporting Information, Table S4 summarizes the reported experimental values for the geometries (Å, deg), electron affinities, and ionization energies in eV.

F. SnHX (X = F, Cl, Br, and I). To assess the effect of halogen substituents for the SnHX series, X = F, Cl, Br, and I, the EA_{ad}, $EA_{ad(ZPVE)}$, EA_{vert}, VDE, E_{IE}, and singlet−triplet splittings are compared to those for the neutral $^1A_1$ state of the SnH_2 molecule. From the ground state $^1A'$ SnHF to its corresponding $^2A''$ anion the increase in the Sn−H and Sn−F bond lengths are 0.062 Å and 0.126 Å (B3LYP), respectively, with a

dx.doi.org/10.1021/ic201389y | Inorg. Chem. 2012, 51, 851−863

small decrease of 0.1° in the divalent angle. From the neutral ^{1}A′ SnHF to its cationic counterpart, shorter bond distances 0.004 Å (Sn−H) and 0.091 Å (Sn−F) are found, accompanying a large increase of 17.7° (B3LYP) in the divalent angle. With respect to SnH_2, monofluoro substitution increases the $EA_{ad(ZPVE)}$ by 0.14 eV, the EA_{vert} by 0.07 eV, and VDE by 0.24 eV. It is predicted that there is a general increase in the electron affinity values as the halogen changes from F → I.

The disubstituted stannylenes show greater abilities to bind an electron compared to the unsymmetrically halosubstituted SnHX (X = F, Cl, Br, and I) stannylenes. For the fluoro, chloro, bromo, and iodo substituents, the $EA_{ad(ZPVE)}$ increase in the order SnH_2 < SnHX < SnX_2, as observed in Table 2. The effect of electron-withdrawal by these halogens is thus rationalized. However, in the case of the fluoro substituent an increase in $EA_{ad(ZPVE)}$ is predicted, in contrast to the observation made[36] for the germylene derivatives from GeH_2 → GeHX (F → Cl → Br → I). A significant dip in the electron affinity is predicted from GeH_2 (1.18 eV) → GeHF (1.10 eV) → GeF_2 (0.98 eV), in contrast to that found for the stannylenes, SnH_2 (0.97 eV) → SnHF (1.09 eV) → SnF_2 (1.16 eV). The incremental $EA_{ad(ZPVE)}$ changes for the SnHX series (X = H, F, Cl, Br, and I) are 0.12, 0.43, 0.04, and 0.21 eV (B3LYP). An unexpected decrease is predicted for the fluoro substituent in the germylene, where the electronegativity of the germanium atom is one of the contributing factors accounting for π-donation from the fluoro substituent. The same trend does not account for the analogous substitution of one fluorine atom in the SnH_2 molecule. It is noted that the singlet−triplet splittings for the series of monosubstituted stannylenes SnHX (X = F, Cl, Br, and I) are lower than those for their corresponding disubstituted SnX_2 molecules.

G. SnFCl, SnFBr, SnFI, SnClBr, SnClI, and SnBrI. It is seen that the ^{2}A′ ground states of the $SnFI^+$, $SnClI^+$, and $SnBrI^+$ cations show unusual structures, with longer Sn−I bond distances and strikingly smaller divalent bond angles compared to their triplet counterparts, as shown in Figure 2.

The replacement of one fluorine atom in SnF_2 by a chloro substituent raises the $EA_{ad(ZPVE)}$ by 0.46 eV, the EA_{vert} by 0.43 eV, and the VDE by 0.51 eV (BHLYP). Conversely, substitution of one chlorine atom in $SnCl_2$ by a fluoro substituent decreases the $EA_{ad(ZPVE)}$ by 0.39 eV, the EA_{vert} by 0.37 eV, and the VDE by 0.41 eV (BHLYP). This general trend for the increase in $EA_{ad(ZPVE)}$ is also seen in going from SnF_2 to SnFI by 0.78 eV. The substitution of one bromine atom into $SnCl_2$ raises the $EA_{ad(ZPVE)}$ by only 0.02 eV, the EA_{vert} by 0.02 eV, and the VDE by 0.03 eV. Chlorine atom substitution into $SnBr_2$ decreases $EA_{ad(ZPVE)}$ by 0.03 eV, EA_{vert} by 0.03 eV, and the VDE by 0.02 eV (BHLYP). It is observed from Table 2 that in the presence of a fluorine atom (SnFCl, SnFBr, and SnFI), the abilities of these species to bind an extra electron are smaller compared to those unsymmetrical tin derivatives containing chlorine, bromine, and iodine atoms (SnClBr, SnClI, and SnBrI). This is interesting because this is contrary to the accepted electronegativities of the halogen atoms.

H. XSnR (X = H, F, Cl, Br, and I; R = CH_3, SiH_3, GeH_3, and SnH_3). Substitution of one H atom by a methyl group in SnH_2 shows a consistent decrease in the $EA_{ad(ZPVE)}$ by 0.14 eV, the EA_{vert} by 0.15 eV and the VDE by 0.12 eV. In going from $HSnCH_3$ → $FSnCH_3$, $EA_{ad(ZPVE)}$, EA_{vert}, and VDE increase by 0.08, 0.04, and 0.16 eV (B3LYP), respectively. Consistent with the theoretical $EA_{ad(ZPVE)}$ values for the series of silylenes and germylenes, the presence of one methyl substituent is accompanied by a significant dip in the electron affinities compared to that effected by one fluorine atom. In going from $HSnCH_3$ to $HSnSiH_3$, there is an increase of 0.484 Å in the Sn−C → Sn−Si bond distance. In contrast, while moving from Sn−Si → Sn−Ge → Sn−Sn the increases are only 0.027 Å and 0.210 Å. Of course this is consistent with the understanding that the greatest periodic differences among main group elements are between the first and the second rows.

To allow a comparative analysis of the halogen species, the electron affinities for $XSnSiH_3$ are examined for X = H, F, Cl, Br, and I. Relative to $HSnSiH_3$, fluorine replacement of the hydrogen atom at the divalent center increases $EA_{ad(ZPVE)}$ by 0.11 eV, EA_{vert} by 0.07 eV, and VDE by 0.18 eV. To compare the effect of the fluoro and silyl substituents, the $EA_{ad(ZPVE)}$ values of SnHF = 0.99 eV and $HSnSiH_3$ = 1.43 eV (BHLYP) are considered. There is a pronounced change in $EA_{ad(ZPVE)}$ with replacement of the fluoro substituent by the electron donating $-SiH_3$ group, as the positive charge density of the central atom decreases. Hence the ability of the $XSnSiH_3$ species to accommodate an extra electron is greater compared to the $XSnCH_3$ family.

The addition of an extra electron to the ^{1}A neutral ground state $HSnGeH_3$ shows only small structural changes. The optimized ^{3}A″ triplet state of $HSnGeH_3$ shows a decrease in the singlet Sn−Ge bond length by 0.076 Å and a large increase in the H−Sn−Ge bond angle of 31.2°. Substitution of one hydrogen atom in SnH_2 by a $-GeH_3$ moiety increases the electron affinity by 0.61 eV, in contrast to the analogous replacement by a methyl group, which decreases the electron affinity. The $EA_{ad(ZPVE)}$ values for $HSnGeH_3$ range from 1.45 (BLYP) to 1.59 eV (B3LYP). The EA_{vert} values for $HSnGeH_3$ are 1.32, 1.31, and 1.45 eV with the BHLYP, BLYP, and B3LYP functionals, respectively, are larger compared to $HSnCH_3$ - with values from 0.60 eV (BLYP) to 0.75 eV (B3LYP). Substitution of the hydrogen in $HSnGeH_3$ molecule by halogens at the divalent center, increases the $EA_{ad(ZPVE)}$ from 1.46 eV (H) → 1.57 eV (F) → 1.90 eV (Cl) → 1.92 eV (Br) → 2.13 eV (I).

The equilibrium geometries of the $XSnSnH_3$ (X = H, F, Cl, Br, and I) species are displayed in Figure 3 and Supporting Information, Figures S30−S33. For the $HSnSnH_3$ molecule, the $EA_{ad(ZPVE)}$, EA_{vert}, and VDE increase by 0.77, 0.65, and 0.88 eV (BHLYP), respectively, compared with SnH_2. The singlet−triplet splittings for $HSnSnH_3$ range from 0.76 eV (BHLYP) to 0.90 eV (BLYP). The $EA_{ad(ZPVE)}$ values increase from 1.73 eV ($HSnSnH_3$) to 2.31 eV ($ISnSnH_3$). A similar trend is observed for the EA_{vert} and VDE values, in the ranges 1.54−2.07 eV and 1.83−2.50 eV, respectively. An increase in the electron affinity is observed upon replacement of the hydrogen atom (attached at the divalent center) by a fluoro substituent for the stannylene family, in contrast to the decrease in the $EA_{ad(ZPVE)}$ observed for the germylene analogues 1.55 eV ($HGeGeH_3$) → 1.50 eV ($FGeGeH_3$).[36] For the carbene,[34] silylene,[35] and germylene[36] analogues, the effect of methyl or fluoro substitution in decreasing the $EA_{ad(ZPVE)}$ is substantial. For the stannylene species the same trend is observed with $-CH_3$ substitution, but an increase in the electron affinities is predicted when one hydrogen atom is replaced by a fluoro substituent.

I. SnR_2 (R = CH_3, SiH_3, GeH_3, and SnH_3). It was established earlier that for the neutral species silylene, $Si(CH_3)_2$,[35] and germylene, $Ge(CH_3)_2$,[36] congeners there is no C_{2v} symmetry equilibrium structure. Similarly, for the $Sn(CH_3)_2$ molecule in Figure 4 no C_{2v} but C_1 point group minimum is found on the potential energy surface. The addition of an extra electron

dx.doi.org/10.1021/ic201389y | Inorg. Chem. 2012, 51, 851−863

to $Sn(CH_3)_2$ shows an increase in the Sn−C bond length by 0.077 Å, with a corresponding decrease in the C−Sn−C bond angle of 0.5°, as well as an increase in the C−H bond length of 0.006 Å, with the dihedral angle Φ(C−Sn−C−H) = 180°. Dewar's MNDO investigation[61] of the organotin(II) molecule, dimethylstannylene $Sn(CH_3)_2$, predicted an Sn−C bond length of 2.027 Å (here BHLYP 2.210 Å) and divalent angle of 99.1° (here 93.0°). The dipole moment was predicted here to be 2.4 D and the ionization energy to have a value of 9.63 eV. In more recent research, the predicted value for the zero point corrected electron affinity for $Si(CH_3)_2$ was 0.38 eV,[35] and for $Ge(CH_3)_2$ 0.46 eV[36] while that predicted here for $Sn(CH_3)_2$ is 0.56 eV. The $EA_{ad(ZPVE)}$ value, on substitution of the hydrogen atoms by two methyl groups in SnH_2, decreases by 0.29 eV with the BHLYP functional. The predicted $Sn(CH_3)_2$ EA_{vert} and VDE values are 0.46 and 0.59 eV, respectively. Substitution of one methyl group in SnH_2, decreases the $EA_{ad(ZPVE)}$ by 0.14 eV, whereas disubstitution further decreases the electron affinity by 0.15 eV.

Similar to the monosubstitution of an $-SiH_3$ group into SnH_2, disubstitution causes an increase in $EA_{ad(ZPVE)}$, EA_{vert}, and VDE by 0.97, 0.86, and 1.08 eV, respectively. In the case of $Sn(SiH_3)_2$, compared to $Sn(CH_3)_2$ the $EA_{ad(ZPVE)}$ increases by 1.24 eV, the EA_{vert} by 1.14 eV, and the VDE by 1.32 eV. The lower predicted $EA_{ad(ZPVE)}$ values indicate that the electron-donor ability of the methyl groups causes the electron density near the central tin atom to increase. Hence, the inductive effect is more pronounced in the presence of two methyl groups. Similar to the silylene and germylene analogues, $Sn(CH_3)_2$ can also bind an extra electron, though weakly, with $EA_{ad(ZPVE)}$ = 0.56 eV. Compared to SnH_2, $-SnH_3$ disubstitution increases the $EA_{ad(ZPVE)}$ substantially by 1.32 eV, EA_{vert} by 1.11 eV, and VDE by 1.49 eV. The theoretical singlet−triplet splitting for $Sn(SnH_3)_2$ ranges from 0.47 (BHLYP) to 0.66 eV (BLYP). A larger singlet−triplet gap is observed for $Sn(CH_3)_2$ relative to the silyl, germyl, and stannyl substituted systems. Following methyl, the $-SiH_3$, $-GeH_3$, and $-SnH_3$, groups behave similarly and increase the germylene electron affinities. This is yet another example of the "great divide" between the first and second row main group elements.

J. Unsymmetrical RSnR′ (R; R′ = CH_3, SiH_3, GeH_3, and SnH_3). All predicted zero-point corrected electron affinities values for the methyl containing structures, $RSnSiH_3$, $RSnGeH_3$, and $RSnSnH_3$ (R = $-CH_3$) are observed to be lower compared to those where R = $-SiH_3$, $-GeH_3$, and $-SnH_3$. The $-SiH_3$, $-GeH_3$, and $-SnH_3$ moieties behave similarly and increase the stannylene electron affinities compared to the $-CH_3$ substituent. This demonstrates that the Sn−Si, Sn−Ge, and Sn−Sn bonds are relatively better σ acceptors than is the Sn−C bond. The conventionally staggered conformers for the $Sn(CH_3)_2$, $Sn(SiH_3)_2$, $Sn(GeH_3)_2$, and $Sn(SnH_3)_2$ molecules are favored over the eclipsed structures, because of repulsive exchange interactions between the electrons of the $-CH_3$, $-SiH_3$, $-GeH_3$, and $-SnH_3$ groups, respectively. This may be correlated with the electronegativities of C, Si, Ge, and Sn and the increasing atomic radii, as well as the donor abilities of the $-CH_3$, $-SiH_3$, $-GeH_3$, and $-SnH_3$ groups. The EA_{vert} values for the species containing one $-CH_3$ moiety are seen to be lower than those for the $-SiH_3$ and $-GeH_3$ groups, namely, 1.10 eV [CH_3SnSiH_3] to 1.78 eV [GeH_3SnSnH_3]. In an analogous manner, the VDE values increase from 1.31−2.16 eV, respectively.

IV. DISCUSSION

This section analyses the trends in the properties of the stannylene derivatives to elucidate the synergistic variations in the geometries, electron affinities, ionization energies, and singlet−triplet gaps.

The trends in the geometric parameters and predicted energetics with respect to the change in the standard Pauling electronegativities:[62] χ_F = 3.98; χ_{Cl} = 3.16; χ_{Br} = 2.96; χ_I = 2.66, χ_C = 2.55, χ_H = 2.20, χ_{Ge} = 2.01, χ_{Sn} = 1.96, and χ_{Si} = 1.90 are fairly regular. Analysis of all the halo-substituted stannylenes, in conjunction with the substituent electronegativities reveals a trend generally consistent with their silicon[35] and germanium[36] analogues. There is the inevitable expected increase in the bond lengths from SnH_2 to SnI_2 as a result of an increase in the size of the halogen atoms (F < Cl < Br < I) bonded to the divalent tin center. For the neutral singlet ground states, SnX_2 (X = H, F, Cl, Br, and I) having C_{2v} point group, the highest occupied molecular orbital (HOMO) is of a_1 symmetry corresponding to the lone pair of electrons lying in the molecular plane. This lone pair of electrons "occupies" a large space resulting in SnX_2^+ bond angles less than 120° for the singlet ground states. The increase in the divalent angles (I > Br > Cl > F > H) is also a consequence of the size of the halogen atom; hence the larger the halogens, the greater is the repulsion between them. Figures 5−7 summarize the effects of halogen substituents on the zero-point corrected electron affinities, ionization energies and singlet−triplet splittings.

Consider the influence of a substituent on the equilibrium bond distances and bond angles for the SnXY series (X; Y = H, F, Cl, Br, and I). There is a fairly regular trend in the neutral singlet geometries with respect to the substituent electronegativity. The predicted geometries of the unsymmetrical SnXY (X = H,

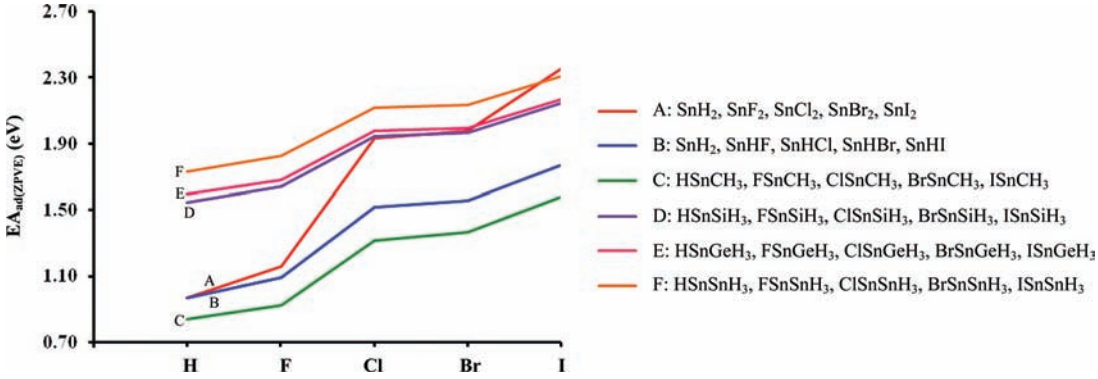

Figure 5. Graph of zero-point corrected electron affinities (eV) (B3LYP) versus substituent.

dx.doi.org/10.1021/ic201389y | Inorg. Chem. 2012, 51, 851−863

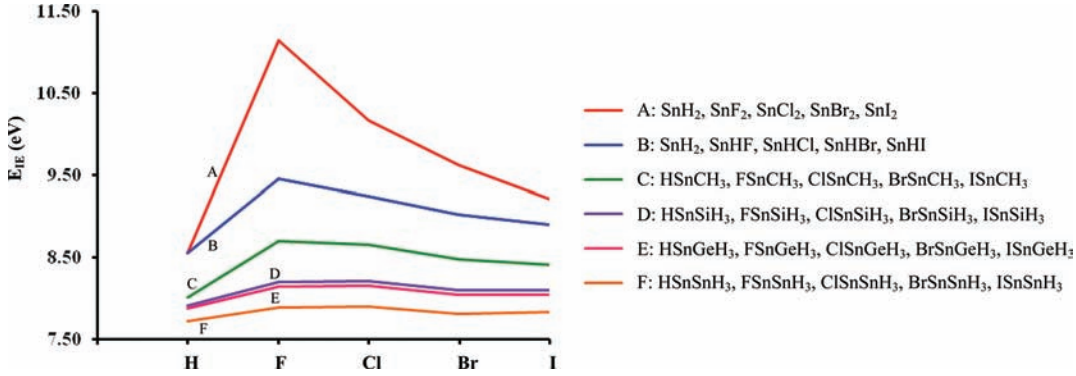

Figure 6. Graph of ionization energy (eV) (B3LYP) versus substituent.

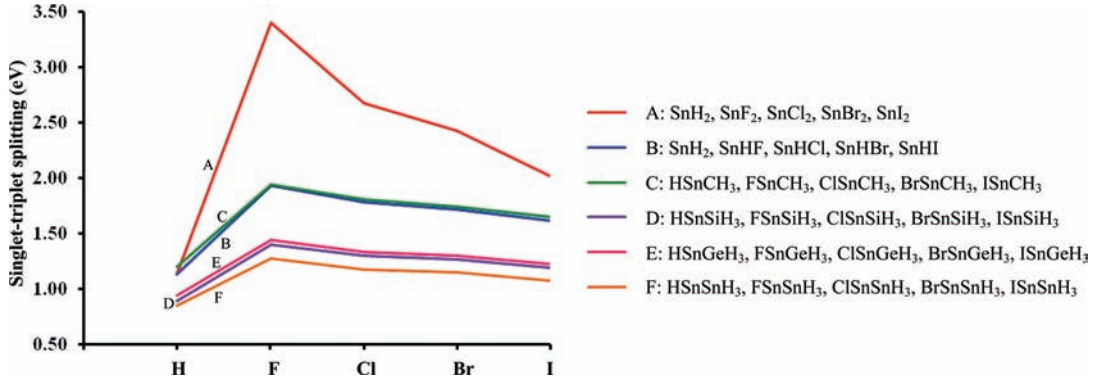

Figure 7. Graph of singlet−triplet splitting (eV) versus substituent.

F, Cl, Br, and I) species show that there is substantial increase in the Sn−F, Sn−Cl, Sn−Br, and Sn−I bond distances as a function of the electronegativity of the adjacent Y substituent. For fixed X, in the series of stannylenes, a synergistic effect is observed with a decrease in the electronegativities of the halogen from F → I, reflecting the changes in the bond distances and bond angles.

The increase in the divalent angle by ∼20°−30° from the neutral singlet ground state structure to its corresponding low-lying triplet ground state, can be regarded as resulting from a decrease in the valence shell electron repulsion upon transfer of an electron from the in-plane HOMO of the singlet to its out-of-plane triplet state. With an increase in the bond angle there is an increase in the s-character of the bonding orbitals. There is also a substituent effect in that the p-character of these bonding orbitals is enhanced by an increase in the substituent electronegativity, consistent with Bent's rule.[63] Bond lengths should increase with increasing p-character of the bonding orbitals and with increasing substituent size. For the same substituent X, the Sn−X bond length decreases in the triplet state reflecting greater s-character of the bonding orbitals accompanying the larger divalent angle. But an opposite effect may be explained by a lower degree of $Sn^{\delta+}-X^{\delta-}$ polarization with the deshielding of the tin nucleus upon transfer of an electron from the HOMO of the singlet state (the HOMO has considerable s-character) to its lowest unoccupied molecular orbital (LUMO) (with no s-character) in the triplet state. These opposing factors explain the much smaller differences between bond lengths compared with differences between bond angles of the corresponding singlet and triplet states.

The triplet bond lengths and bond angles also exhibit similarly, although less pronounced trends. The large changes from the neutral ground state geometries to their cations and triplet states also accounts for the change in the vibrational progressions in their IR spectra for the C_{2v} symmetry SnX_2 (X = H, F, Cl, Br, and I) molecules. This is mostly reflected in the bending mode rather the stretching modes. Their dipole moments (Debye) are reported in Table 1. The significant decreases in the monosubstituted H−Sn−X (X = F, Cl, Br, and I) divalent bond angle, compared to the symmetrical SnX_2 (X = F, Cl, Br, and I), species results from the smaller size and low electronegativity of the hydrogen atom. Effectively, there is an observed stabilization of the singlet structures of stannylenes by halogen substituents. The structures of the $^2A_1$ ground states of SnX_2^+ cations are very close to the geometrical parameters of their corresponding $^3B_1$ low-lying triplet states, because of the removal of an electron from the a_1 orbital in both cation and triplet cases.

The predicted singlet−triplet splitting values for the halo-substituted stannylenes can be understood in terms of the influence of the charge on the divalent tin center and π-donation from the substituent. The relationship between charge and electronegativity indicates that σ-donation and π-backbonding act synergistically in determining the value of the singlet−triplet gap. The relative trends in the predicted singlet−triplet gaps are in fact correlated with the electronegativity of the substituent, as observed from Table 4, where, with an increase in the electronegativity of the substituent, the singlet−triplet splitting increases. There is greater stabilization of a singlet state by π-donor substituent than of the corresponding triplet state, because the Sn 5p orbital is empty in the singlet but singly occupied in the triplet. The observed trends also show that the electron-withdrawing substituent inductively favors the σ nonbonding orbital by increasing the s character. The change in hybridization between the σ^2p^0 (singlet) and σ^1p^1 (triplet)

dx.doi.org/10.1021/ic201389y | Inorg. Chem. 2012, 51, 851−863

increases the energy gap. Singlet stannylenes have smaller bond angles than triplets, with more tin p character leading to stronger σ bonding and stabilization of the singlet. Hence, we understand the singlet−triplet gaps for the dihalosubstituted stannylenes to be significantly larger in comparison to the monosubstituted molecules. Electronegative substituents withdraw electron density from the divalent tin center, making it more positively charged; consequently, the increase in charge makes the tin atom a better π-acceptor. The increasing electron affinities for the series SnH_2 < SnHX < SnX_2, indicate that electron-withdrawal is the major effect.

The irregularity of the predicted bond angles for tin dihydrides SnH_2 and the mono substituted stannylenes is due to the low steric factor of the hydrogen atom(s). The exception is observed for the monohalostannylenes, HSnY molecules, where the Sn−H bond lengths and the bond angles decrease monotonically with an increase in the electronegativity of substituent Y. Their corresponding triplet species exhibit similar variations in the bond lengths and bond angles. The p character of the bonding orbitals is augmented with an increase in the electronegativity of the second substituent and reflected in the predicted equilibrium geometries. The significant increase in the positive Mulliken atomic charges of the divalent tin center from (+0.40e) to (+0.51e) with monofluoro substitution enhances the polarity of the Sn−F bond as well as the repulsion between the negatively charged fluorine atom (−0.51e) and the hydrogen atom (−0.20e). The σ Sn−F bond is thus more polar than the Sn−Cl, Sn−Br, and Sn−I bonds, supported by predicted charges on the Sn and halogen atoms (+0.59e,−0.38e), (+0.57e,−0.37e), and (+0.50e,−0.34e), respectively. This implies that polarity is one of the factors affecting the ability to accommodate an extra electron. This polarizability argument explains the poorer σ withdrawing abilities of the Sn−Cl, Sn−Br, and Sn−I bonds and the less effective donor abilities of the nonbonding electron pairs on these halogen substituents. This confirms that there are no large differences in the withdrawing abilities of the Sn−Cl, Sn−Br, and Sn−I bonds. Contrary to the order of the halogen electronegativities, which decrease in the order F > Cl > Br > I, the electron affinities increase in the opposite order.

For the SnX_2 (X = H, F, Cl, Br, and I) molecules, the standard Pauling electronegativities of the halogen atoms and their increasing sizes are reflected in the HOMO energies. For the highly electronegative fluorine atom (χ_F = 3.98), the contribution of the tin s orbital to the a_1 HOMO energy in the neutral singlet state of SnF_2 is lowered compared to the SnH_2 molecule. This increases the LUMO−HOMO gap by favoring electron pairing; hence, the singlet is the ground state. While the b_1 orbital is the ground state LUMO, it is the singly occupied molecular orbital (SOMO) in the lowest-lying triplet state. This is because one of the electrons from the singlet a_1 orbital is promoted to the b_1 orbital, which is an out-of-plane nonbonding orbital, comprising the tin out-of-plane p orbital and the out-of-plane p orbitals of the halo-substituent. The a_1 populations are found as SnF_2: $5s^{1.84}5p^{0.58}$; $SnCl_2$: $5s^{1.89}5p^{0.90}$; $SnBr_2$: $5s^{1.90}5p^{1.03}6p^{0.01}$; SnI_2: $5s^{1.92}5p^{1.26}6p^{0.01}$. With a decrease in the electronegativities of the halogens down the periodic table, the contribution of the tin s orbitals to the a_1 molecular orbital decreases, concomitantly raising the a_1 orbital energy. In the lowest-lying triplet state it is noted that a decrease in the electronegativity of the halogen substituents and an increase in their sizes causes the energy of the out-of-plane p orbital on the halogen to increase. The overlapping of these orbitals with the tin p orbital is diminished, and the antibonding nature of the b_1 orbital is decreased. Therefore, in going from F → Cl → Br → I, the separation between the a_1 and b_1 orbitals becomes smaller and the singlet−triplet energy gaps decrease.

The electronic excitation from the $^1A_1$ neutral ground state to the $^3B_1$ lowest-lying triplet state arises from the promotion of an electron from the a_1 orbital to an orbital of b_1 symmetry the latter being the out-of-plane atomic p orbital of the divalent tin atom. As a result, of the valence shell electrons in the molecular plane, only one electron remains in a_1 at the tin center, leading to a large decrease in the repulsion. Consequently, the divalent bond angles of the neutral triplet state molecules are wider compared to their respective neutral singlet states. There is stabilization of the singlet electronic states of the stannylenes by halogen substituents, since both the σ-withdrawing and π-donating abilities of the halogen increase with rising electronegativity. Electron-withdrawing substituents occupy orbitals of increasing p character, compared to electron-donating substituents, hence inductively stabilizing the nonbonding pair of electrons in the singlet ground state, augmenting the s character of that orbital. The electron π-donating ability of the halogen also favors the singlet state by donating electron density to the empty p orbital.

The SnX_2/SnXY and XSnR/SnR_2/RSnR′ (X, Y = H, F, Cl, Br, I, and R, R′ = CH_3, SiH_3, GeH_3, SnH_3) molecules have strikingly smaller divalent bond angles compared to their germylene analogues, which may be attributed to the smaller electron density on Sn compared to the divalent germanium center. The contribution of the tin-halogen overlap is less and hence stannylene derivatives have ionic characteristics. Analyzing the SnF_2 molecule, it is expected to be more ionic than GeF_2 because of the change in the valence populations of the divalent central atoms, Ge: [core] $4s^{1.82}4p^{0.6936}$ and Sn: [core] $5s^{1.84}5p^{0.58}$ respectively. Accordingly, the large LUMO−HOMO gap of singlet $^1A_1$ SnF_2 = 5.45 eV (B3LYP) favors its neutral ground electronic state with respect to its lowest-lying triplet state. At 3.40 eV SnF_2 has the largest singlet−triplet gap in the series.

The π-donation from the halogen substituents is correlated with the singlet−triplet gaps for SnX_2, but there is an inverse correlation with bond angle. The variation in the bond angle is due to a change in the hybridization of the central atom. For the SnX_2 (X = F, Cl, Br, and I) series, the resulting increase in p-character in the nonbonding σ-orbitals in turn leads to generally lower singlet−triplet gaps. It may be seen from Table 2 that fluorine does not decrease the $EA_{ad(ZPVE)}$ value in going from HSnX → FSnX and HSnR → FSnR (X = H, R = CH_3, SiH_3, GeH_3, and SnH_3), as found for the carbene, silylene, and germylene analogues.

As one descends group IV in the periodic table, for the HSnR (R = CH_3, SiH_3, GeH_3, SnH_3) series a fairly regular trend in the electron affinities, ionization energies, and singlet−triplet gaps energies is seen. From C → Si → Ge → Sn, the Sn−R internuclear distance inevitably increases; this causes the electron donor ability of the −R moiety to vary considerably in the series $HSnCH_3 \gg HSnSiH_3 > HSnGeH_3 > HSnSnH_3$, where the predicted $EA_{ad(ZPVE)}$ increase from C → Si → Ge → Sn, namely, 0.71, 1.43, 1.46, and 1.62 eV, respectively. This shows that the Sn−Si, Sn−Ge, and Sn−Sn bonds are relatively better σ acceptors than the Sn−C bond. The effect of electron-donating methyl group is significantly enhanced compared to the $-SiH_3$, $-GeH_3$, and $-SnH_3$ groups. The trend observed for the $-SiH_3$, $-GeH_3$, and $-SnH_3$ moieties is notably comparable to that observed for the $-CH_3$ moiety. In keeping with Larkin

dx.doi.org/10.1021/ic201389y | Inorg. Chem. 2012, 51, 851−863

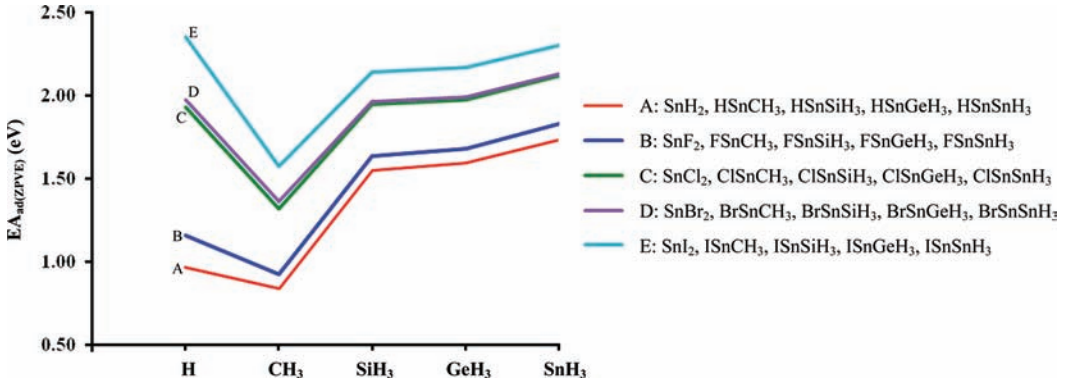

Figure 8. Graph of zero-point corrected electron affinities (eV) versus H, $-CH_3$, $-SiH_3$, $-GeH_3$, and $-SnH_3$ substituents.

and Schaefer's findings[35] for the silicon analogues, the methyl substituent(s) significantly decrease the electron affinities for the mono- and di- substituted tin hydride. Consistent with the electron affinities for the silicon analogues, the methyl substituents reduce the different forms of electron affinities compared to the analogous fluorine systems. Similarly, a halogen atom attached to the divalent center M = C, Si, Ge, and Sn for the series $HSnMH_3$ has the same effect as that predicted in the electron affinities for SnX_2 (X = F, Cl, Br, I) when going from F → Cl → Br → I. Figure 8 presents a graphical representation of the $EA_{ad(ZPVE)}$ values as a function of the H, $-CH_3$, $-SiH_3$, $-GeH_3$, and $-SnH_3$ substituents.

V. CONCLUSIONS

In this research, we have investigated the structures, electron affinities, ionization energies, and singlet−triplet gaps of the SnX_2/SnXY and XSnR/SnR_2/RSnR′ species (X; Y = H, F, Cl, Br, I and R; R′ = CH_3, SiH_3, GeH_3 and SnH_3). This study includes many yet unknown but potentially important species. Four types of electron affinities are computed: EA_{ad}, $EA_{ad(ZPVE)}$, EA_{vert}, and VDE. The BHLYP functional which incorporates the largest fraction of the Hartree−Fock method[39] predicts more reliable geometries, harmonic vibrational wavenumbers, and electron affinities in comparison with the limited available experiments. It is concluded that dimethylstannylene binds an electron, though more weakly compared to its silicon and germanium congeners, lying in the order 0.38 eV [$Si(CH_3)_2$] < 0.46 eV [$Ge(CH_3)_2$] < 0.56 eV [$Sn(CH_3)_2$]. The abilities of the stannylene derivatives to bind an extra electron range from 0.56 eV [$Sn(CH_3)_2$] to 2.43 eV [SnI_2] with the BHLYP functional. The computed E_{IE} values range from 7.33 eV [$Sn(SnH_3)_2$] to 11.15 eV [SnF_2], while the singlet−triplet splittings range from 0.60 eV [$Sn(SnH_3)_2$] to 3.40 eV [SnF_2]. For the present tin-containing compounds it is observed that the replacement of the hydrogen atom in SnH_2 and $HSnMH_3$ (M = C, Si, Ge, and Sn) by a fluoro substituent increases the electron affinities. The trend is apparent: the largest singlet−triplet splitting appears in the difluorostannylene for all SnX_2 (X = halogen) and decreases toward the iodides. As established earlier for $Si(CH_3)_2$[35] and $Ge(CH_3)_2$,[36] we find here no neutral structure of C_{2v} symmetry $Sn(CH_3)_2$ molecule to be a minimum on the singlet potential energy surface. The SiH_3, GeH_3, and SnH_3 groups behave similarly and increase the stannylene electron affinities versus CH_3 substitution.

■ ASSOCIATED CONTENT

Ⓢ Supporting Information

Further details are given about the equilibrium geometries, theoretical harmonic vibrational wavenumbers, vertical electron affinities and detachment energies. This material is available free of charge via the Internet at http://pubs.acs.org.

■ AUTHOR INFORMATION

Corresponding Author

*E-mail: ramchemi@intnet.mu (P.R.), fri@uga.edu (H.F.S.).

■ ACKNOWLEDGMENTS

A.B. acknowledges financial support from the Mauritius Tertiary Education Commission (TEC). In Georgia, this research was supported by the National Science Foundation, Grant CHE-1054286. We acknowledge the use of facilities at the University of Mauritius and Center for Computational Quantum Chemistry (CCQC). We thank Dr Yaoming Xie and Dr Qiang Hao for skillful assistance. We also thank all reviewers for their helpful comments on improving the manuscript.

■ REFERENCES

(1) Bazargan, S.; Heinig, N. F.; Pradhan, D.; Leung, K. T. *Cryst. Growth Des.* **2011**, *11*, 247.
(2) Hahn, N. T.; Mullins, C. B. *Chem. Mater.* **2010**, *22*, 6474.
(3) Otero-de-la-Roza, A.; Luaa, V. *J. Chem. Theory Comput.* **2010**, *6*, 3761.
(4) Merrill, W. A.; Wright, R. J.; Stanciu, C. S.; Olmstead, M. M.; Fettinger, J. C.; Power, P. P. *Inorg. Chem.* **2010**, *49*, 7097.
(5) Matioszek, D.; Katir, N.; Saffon, N.; Castel, A. *Organometallics* **2010**, *29*, 3039.
(6) Semenov, S. N.; Blacque, O.; Fox, T.; Venkatesan, K.; Berke, H. *Organometallics* **2010**, *29*, 6321.
(7) Jung, B. J.; Tremblay, N. J.; Yeh, M.-L.; Katz, H. E. *Chem. Mater.* **2010**, 568.
(8) Meng, X.; Geng, D.; Liu, J.; Banis, M. N.; Zhang, Y.; Li, R.; Sun, X. *J. Phys. Chem. C* **2010**, *114*, 18330.
(9) Fukawa, T.; Lee, V. Y.; Nakamoto, M.; Sekiguchi, A. *J. Am. Chem. Soc.* **2004**, *126*, 11758.
(10) Lee, V. Y.; Fukawa, T.; Nakamoto, M.; Sekiguchi, A.; Tumanskii, B. L.; Karni, M.; Apeloig, Y. *J. Am. Chem. Soc.* **2006**, *128*, 11643.
(11) Setaka, W.; Hirai, K.; Tomioka, H.; Sakamoto, K.; Kira, M. *J. Am. Chem. Soc.* **2004**, *126*, 2696.
(12) Arp, H.; Baumgartner, J.; Marschner, C.; Müller, T. *J. Am. Chem. Soc.* **2011**, *133*, 5632.
(13) Dickschat, J. V.; Urban, S.; Pape, T.; Glorius, F.; Hahn, F. E. *Dalton Trans.* **2010**, *39*, 11519.

(14) Brendler, E.; Wächtler, E.; Heine, T.; Zhechkov, L.; Langer, T.; Pöttgen, R.; Hill, A. F.; Wagler, J. *Angew. Chem., Int. Ed.* **2011**, *50*, 4696.
(15) Boganov, S. E.; Egorov, M. P.; Faustov, V. I.; Nefedov, O. M. The Chemistry of Organic Germanium, Tin and Lead Compounds; Raoppoport, Z., Ed.; John Wiley & Sons: New York, 2002; Vol. 2, Part 1, pp 749−841.
(16) Zhou, D.; Reiche, C.; Soderquist, J. A.; Gaspar, P. P. *Organometallics* **2009**, *28*, 2595.
(17) Becerra, R.; Gaspar, P. P.; Harrington, C. H.; Leigh, W. J.; Vargas-Baca, I.; Walsh, R.; Zhou, D. *J. Am. Chem. Soc.* **2005**, *127*, 17469.
(18) Albertin, G.; Antoniutti, S.; Castro, J. *Organometallics* **2010**, *29*, 3808.
(19) Lee, E. P. F; Dyke, J. M.; Mok, D. K. W.; Chow, W.-K.; Chau, F.-T. *J. Chem. Phys.* **2007**, *127*, 024308.
(20) Lee, E. P. F; Dyke, J. M.; Chow, W.-K.; Mok, D. K. W.; Chau, F.-T. *J. Phys. Chem. A* **2007**, *111*, 13193.
(21) Lee, E. P. F; Dyke, J. M.; Mok, D. K. W.; Chow, W.-K.; Chau, F.-T. *Phys. Chem. Chem. Phys.* **2008**, *10*, 834.
(22) Nasarenko, A. Y.; Spiridonov, V. P.; Butayev, B. S.; Zasorin, E. Z. *J. Mol. Struct.* **1985**, *119*, 263.
(23) Novak, I.; Potts, A. W. *J. Electron Spectrosc. Relat. Phenom.* **1984**, *33*, 1.
(24) Harris, D. H.; Lappert, M. F.; Pedley, J. B.; Sharp, G. J. *J. Chem. Soc., Dalton Trans.* **1976**, 945.
(25) Evans, S.; Orchard, A. F. J. *Electron Spectrosc. Relat. Phenom* **1975**, *6*, 207.
(26) Olbrich, G. *Chem. Phys. Lett.* **1980**, *73*, 110.
(27) Balasubramanian, K. *Chem. Phys. Lett.* **1986**, *127*, 585.
(28) Balasubramanian, K. *J. Phys. Chem.* **1989**, *93*, 6585.
(29) Ricart, J. M.; Rubio, J.; Illas, F. *Chem. Phys. Lett.* **1986**, *123*, 528.
(30) Benavides-Garcia, M.; Balasubramanian, K. *J. Chem. Phys.* **1994**, *100*, 2821.
(31) Escalante, S.; Vargas, R.; Vela, A. *J. Phys. Chem. A* **1999**, *103*, 5590.
(32) Szabados, A.; Hargittai, M. *J. Phys. Chem. A* **2003**, *107*, 4314.
(33) For an introductionto ab initio studies of carbenes, see: O'Neil, S. V.; Schaefer, H. F.; Bender, C. F. *J. Chem. Phys.* **1971**, *55*, 162.
(34) Irikura, K. K.; Goddard, W. A.; Beauchamp, J. L. *J. Am. Chem. Soc.* **1992**, *114*, 48.
(35) Larkin, J. D.; Schaefer, H. F. *J. Chem. Phys.* **2004**, *121*, 9361.
(36) Bundhun, A.; Ramasami, P.; Schaefer, H. F. *J. Phys. Chem. A* **2009**, *113*, 8080.
(37) Frisch, M. J. et al. *Gaussian 03*, Revision C.02; Gaussian Inc.: Wallingford, CT, 2004.
(38) Becke, A. D. *J. Chem. Phys.* **1988**, *38*, 3098.
(39) Becke, A. D. *J. Chem. Phys.* **1993**, *98*, 1372.
(40) Lee, C.; Yang, W.; Parr, R. G. *Phys. Rev. B* **1988**, *37*, 785.
(41) Glendening, E. D.; Reed, A. E.; Carpenter, J. E.; Weinhold, F. *NBO*, Version 3.1.
(42) For pseudopotentials of the Stuttgart-Dresden, see http://www.theochem.uni-stuttgart.de/pseudopotentials/index.en.html.
(43) Huzinaga, S. *J. Chem. Phys.* **1965**, *42*, 1293.
(44) Dunning, T. H.; Hay, P. J. In *Modern Theoretical Chemistry*; Schaefer, H. F., Ed.; Plenum: New York, 1977; Vol. 3, pp 1−27.
(45) Huzinaga, S. *Approximate Atomic Wavefunctions II*; University of Alberta: Edmonton, Alberta, Canada, 1971.
(46) Schafer, A.; Horn, H.; Ahlrichs, R. *J. Chem. Phys.* **1992**, *97*, 2571.
(47) Lee, T. J.; Schaefer, H. F. *J. Chem. Phys.* **1985**, *83*, 1784.
(48) Wang, X.; Andrews, L.; Chertihin, G. V.; Souter, P. F. *J. Phys. Chem. A* **2002**, *106*, 6302.
(49) Wang, X.; Andrews, L. *J. Am. Chem. Soc.* **2003**, *125*, 6581.
(50) Balasubramanian, K. *J. Chem. Phys.* **1988**, *89*, 5731.
(51) Hauge, R. H.; Hastie, J. W.; Margrave, J. L. *J. Phys. Chem.* **1968**, *72*, 3510.
(52) Hauge, R. H.; Hastie, J. W.; Margrave, J. L. *J. Mol. Spectrosc.* **1973**, *45*, 420.
(53) Novak, I.; Potts, A. W. *J. Chem. Soc., Dalton Trans.* **1983**, 2211.
(54) Zmbov, K. F.; Hastie, J. W.; Margrave, J. L. *J. Chem. Soc., Faraday Trans.* **1968**, *64*, 861.
(55) Hastie, J. W.; Zmbov, K. F.; Margrave, J. L. *J. Inorg. Nucl. Chem.* **1968**, *30*, 729.
(56) Dai, D.; AI-Zahrani, M. M.; Balasubramanian, K. *J. Phys. Chem.* **1994**, *98*, 9233.
(57) Pabst, R. E.; Perry, D. L.; Margrave, J. L.; Franklin, J. L. *Int. J. Mass Spectrom. Ion Phys.* **1977**, *24*, 323.
(58) Hirayama, C.; Straw, R. D. *Thermochim. Acta* **1984**, *80*, 297.
(59) Knowles, D. J.; Nicholson, A. J. C.; Swingler, D. L. *J. Phys. Chem.* **1970**, *74*, 3642.
(60) Hilpert, K.; Gingerich, K. A. *Int. J. Mass Spectrom. Ion Phys.* **1983**, *47*, 247.
(61) Dewar, M. J. S.; Friedheim, J. E.; Grady, G. L. *Organometallics* **1985**, *4*, 1784.
(62) Bergmann, D.; Hinze, J. *Angew Chem., Int. Ed. Engl.* **1996**, *35*, 150.
(63) Bent, H. A. *Chem. Rev.* **1961**, *61*, 275.
(64) Leopold, D. G.; Murray, K. K.; Miller, A. E. S.; Lineberger, W. C. *J. Chem. Phys.* **1985**, *83*, 4849.
(65) Harland, P. W.; Thynne, J. C. J. *Int. J. Mass Spectrom. Ion Phys.* **1972**, *10*, 11.
(66) Schwartz, R. L.; Davico, G. E.; Ramond, T. M.; Lineberger, W. C. *J. Phys. Chem. A* **1999**, *103*, 8213.
(67) Murray, K. K.; Leopold, D. G.; Miller, T. M.; Lineberger, W. C. *J. Chem. Phys.* **1988**, *89*, 5442.